

## Isothermal compression of staurolite: A single-crystal study

PAOLA COMODI,<sup>1</sup> MICHELA MONTAGNOLI,<sup>1</sup> PIER FRANCESCO ZANAZZI,<sup>1,\*</sup>  
AND TIZIANA BOFFA BALLARAN<sup>2</sup>

<sup>1</sup>Dipartimento di Scienze della Terra, Università di Perugia, 06100 Perugia, Italy

<sup>2</sup>Bayerisches Geoinstitute, Universität Bayreuth, D-95440 Bayreuth, Germany

### ABSTRACT

The response of staurolite to pressure was studied by single crystal X-ray diffraction (XRD) in a diamond-anvil cell, using crystals with composition:  $(\text{Fe}_{3.365}\text{Zn}_{0.025}\text{Li}_{0.114}\text{Co}_{0.009}\text{Mn}_{0.034})[\text{T2}, \text{M4}] (\text{Al}_2\text{Mg}_{0.307})[\text{M3}] (\text{Al}_{15.491}\text{Fe}_{0.104}^{3+}\text{Mg}_{0.394}\text{Cr}_{0.004}\text{Ti}_{0.07})[\text{M1}, \text{M2}] (\text{Si}_{7.534}\text{Al}_{0.466})[\text{T1}] \text{O}_{48}\text{H}_3$ .

Lattice parameters, measured at various pressure up to 7.264(6) GPa, were fitted using a third-order Birch-Murnaghan equation of state (EoS). The resulting EoS parameters are:  $V_0 = 740.85(7) \text{ \AA}^3$ ,  $K_0 = 180(2) \text{ GPa}$  and  $K' = 4.7(6)$ ,  $a_0 = 7.8723(2) \text{ \AA}$ ,  $K_0 = 189(2) \text{ GPa}$ , and  $K'_a = 4.1(6)$ ,  $b_0 = 16.62453(1) \text{ \AA}$ ,  $K_0 = 179(2) \text{ GPa}$ ,  $K'_b = 6.1(6)$  and  $c_0 = 5.6604(4) \text{ \AA}$ ,  $K_0 = 179(5) \text{ GPa}$ ,  $K'_c = 2(1)$ ; whereas the angle  $\beta$  remained almost constant with increasing pressure. These data suggest an almost isotropic compressibility.

Structural evolution was studied by comparison of structural refinements carried out with data collected at 0.0001, 2.48, 4.15, 5.43, 6.84, and 8.74 GPa. All refinements were made in the *Ccmm* space group. Polyhedral evolution with *P* is a function of occupancy: whereas the T1 tetrahedron and the M1 and M2 octahedra, occupied by Si and Al, are practically incompressible, the T2 tetrahedron, and the M4 and M3 octahedra, only partially occupied principally by Fe (the first two) and by Al (the last), show larger changes as a function of pressure. As a consequence, the two kyanite and Fe-Al hydroxide layers, which can be used to describe the staurolite structure, have different compressibilities.

### INTRODUCTION

Staurolite is a common mineral in metapelitic rocks and occurs rarely in some metabasites. Its structure was determined by Nary-Szabo (1929) in the *Ccmm* space group and later re-investigated by Nary-Szabo and Sasvari (1958), who showed that staurolite has only pseudo-orthorhombic symmetry and that its correct symmetry is monoclinic, *C2/m* space group, with  $\beta \cong 90^\circ$ .

Structural investigation of a large group of natural staurolite samples by Hawthorne et al. (1993a, 1993b, 1993c) showed the complex crystal chemistry of this phase. Fe-rich staurolite may be represented by the formula  $\text{Fe}_{3+4}^{2+[\text{T2}]} \text{Fe}_{0-0.5}^{2+[\text{M4}]} (\text{Al}_2 \square_2)^{[\text{M3}]} \text{Al}_{16}^{[\text{M1}, \text{M2}]} \text{Si}_8^{[\text{T1}]} \text{O}_{48} \text{H}_{2-4}$  in which the various crystallographic sites are indicated in brackets.  $\text{Fe}^{2+}$  may be substituted by Mg, Zn, Mn, and some Al. In Mg-staurolite from Dora Maira, Italy; Hawthorne et al. (1993a) and Koch-Muller et al. (1999) assigned Mg to M4 and reduced the occupancy of T2, in agreement with the general observation that cation coordination tends to increase in high-*P* phases.

Neutron diffraction studies (Stahl et al. 1988) and polarized infrared absorption spectra (Koch-Muller et al. 1995, 1998) have definitely clarified the position of H in the structure. From the pleochroic behavior of the OH vibration, Koch-Muller et al. (1995) concluded that the two hydroxyl groups, OH1 and OH2, are in the (010) plane and have the larger component along *c* and *a*. Caucia et al. (1994) showed that the H content in staurolite changes with the variable occupancy of M3.

The general structure of staurolite may be described as a close-packed oxygen arrangement, but many authors prefer to describe it as an overlap of (010) layers consisting of kyanite  $[\text{Al}_2\text{SiO}_5]$  and Fe-Al-oxide-hydroxide  $[\text{IVAl}_{0.7}\text{Fe}_2\text{O}_2(\text{OH})_2]$  alternating in the (001) plane along the *b* axis (Fig. 1). In kyanite slabs, the octahedral sites are completely occupied by Al + (Fe + Mg) and the tetrahedral sites by Si + Al. The Fe-Al-oxide-hydroxide is based on edge-sharing octahedra, forming a chain of M3 and M4 extending along [001], flanked by  $\text{FeO}_4$

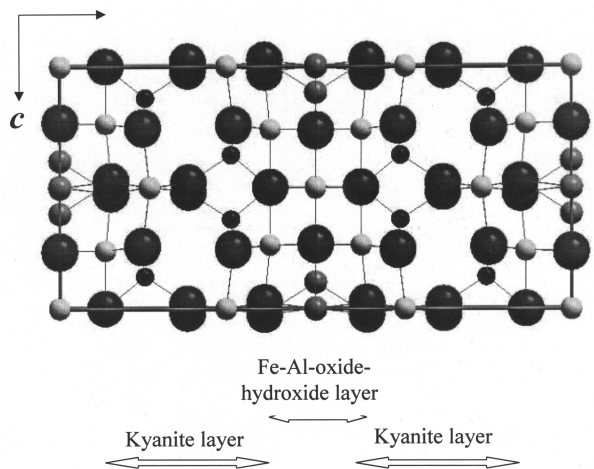


FIGURE 1. The staurolite structure projected along the *a* axis. The alternating of kyanite and Fe-Al hydroxide layers is indicated.

\* E-mail: zanazzi@unipg.it

tetrahedra (T2) sharing faces with the octahedra.

The complete structure of staurolite was derived by Andersson and Hyde (1982) from that of spinel by applying simple crystallographic shear. Shear planes at  $y = 1/4$  and  $y = 3/4$  in the (100) plane, with a translation of  $z + 1/2$  of the spinel structure, generate the staurolite structure. With the shear operation, some octahedra occupied in the spinel structure are lost in the staurolite structure (see Fig. 2 in Ståhl and Legros 1990).

Fe-staurolite is stable between 550 and 700 °C for  $P > 0.15$  GPa (Richardson 1966) and even at lower  $T$  for  $P > 0.9$  GPa (Ganguly 1972). Mg-staurolite with  $Mg/(Mg + Fe + Zn + Co) > 0.5$ , stable between 700 and 1000 °C for  $P > 1.2$  GPa (Schreyer and Chinner 1966), has been found in rocks metamorphosed at pressures greater than 3 GPa (Schreyer 1988).

Experimental studies by Hellman and Green (1978) and others based on natural examples (Gibson 1978) first showed that staurolite is not necessarily confined to pelitic compositions and may exist over a large  $P$ - $T$  range in mafic rocks. Moreover, Hellman and Green (1978) hypothesized that staurolite is important in petrogenetic models of mineralogical changes and melting processes occurring in Benioff zones. Recent experimental petrological studies (Poli and Schmidt 1995) have shown that staurolite is one of the hydrous phases, together with lawsonite, chloritoid, phengite, and zoisite-clinozoisite, that are candidates for the transport of water to pressures higher than that of amphibole breakdown in andesitic and basaltic systems. However, models for water release from subducted slabs need not only thermal models for subduction zones, but also clearly determined experimental phase relationships.

The effect of temperature on staurolite was studied by Gibbons et al. (1981) by the high-temperature powder XRD method. They measured the mean expansion coefficient up to about 500 °C, when dehydroxylation occurred. Caucia et al. (1994), studying structural aspects of the oxidation-dehydrogenation process, showed a decrease in degree of order with  $T$ , approaching orthorhombic symmetry, and oxidation of Fe in the T2 site, with loss of the associated H. However, no data are known on the behavior of staurolite structure with  $P$ . Only Grevel et al. (1998) measured the  $P$ - $V$ - $T$  behavior of an Mg-staurolite from powder diffraction using multi-anvil X-ray apparatus.

The aim of the present study was to determine the structural evolution of Fe-staurolite with  $P$  and to compare its behaviour with that of Mg-staurolite (Grevel et al. 1998).

## EXPERIMENTAL METHODS

A sample from Dervio, Italy, was investigated, which corresponds to no. 28 used in the crystallochemical study of Hawthorne et al. (1993a). Some selected crystals were analysed using an energy dispersive system (EDS) on a scanning electron microscope (SEM). The average composition corresponds to that reported in Hawthorne et al. (1993b):  $(Fe_{3.365}Zn_{0.025}Li_{0.114}Co_{0.009}Mn_{0.034})[T2, M4](Al_2Mg_{0.307})[M3](Al_{15.491}Fe_{0.104}^{3+}Mg_{0.394}Cr_{0.004}Ti_{0.07})[M1, M2](Si_{7.534}Al_{0.466})[T1]O_{48}H_3$ .

Unit-cell parameters were determined with a BGI diamond-anvil cell (DAC) using a Hüber four-circle diffractometer at the Bayerisches Geoinstitut (Germany). High-pressure structure determinations were carried out with a Merrill-Bassett DAC

on a four-circle Philips PW1100 diffractometer at Dipartimento di Scienze della Terra, University of Perugia (Italy).

A staurolite crystal with dimensions of  $110 \times 140 \times 70 \mu m$  (Sample I) was loaded in the BGI DAC, using T301 steel as gasket material and a 4:1 methanol-ethanol mixture as a pressure-transmitting medium, together with a ruby for approximate pressure determination and a quartz crystal as an internal pressure standard. Details of the instrument and the peak-centering algorithms are described by Angel et al. (1997). This mounting allowed us to determine unit-cell parameters of both staurolite and the pressure calibrant in the pressure range 0.0001 and 7.264(6) GPa by the vector-least-squares method (Ralph and Finger 1982). Unit-cell parameters determined by a least-squares fit to the corrected setting angles of reflections showed no deviations from symmetry constrained values greater than one estimated standard deviation. The values of the monoclinic symmetry constrained unit-cell parameters are reported in Table 1.

Before the high-pressure study, geometric and intensity data at ambient conditions were collected with a four-circle, Philips PW1100 diffractometer, using graphite monochromatized  $MoK\alpha$  radiation ( $\lambda = 0.7107 \text{ \AA}$ ). Afterward, the sample was mounted in a Merrill-Bassett DAC using a methanol-ethanol 4:1 mixture as a pressure-transmitting medium and a steel foil, 250  $\mu m$  thick, as gasket material. Pressure was monitored by measuring the wavelength shift of the fluorescence line at 6876  $\text{\AA}$  of  $Sm^{2+}$  ( $Sm:BaFCl$ ), excited by a 100 mW Ar laser and detected by a 100 cm Jarrell-Ash optical spectrometer (Comodi and Zanazzi 1993a). The uncertainties in the pressure measurements were 0.05 GPa. X-ray intensity data sets at 0.0001, 2.48, 4.15, and 5.43 GPa, were obtained using a crystal with dimensions  $120 \times 150 \times 80 \mu m$  (Sample II). A second mounting (Sample III) was tried to achieve higher pressure. Sample III with the same composition as Sample II but smaller dimensions ( $100 \times 110 \times 70 \mu m$ ) was mounted in the DAC and two additional X-ray intensity data sets were collected at 6.84 and 8.74 GPa. Both data sets were collected using a non-bisecting geometry (Denner et al. 1978) and  $2.0^\circ$  width  $\omega$  scan and analyzed with a digital procedure (Comodi et al. 1994) in order to maximize reflection accessibility and minimize attenuation of the X-ray beams by the pressure-cell components. Data were corrected for the pressure-cell absorption by an experimental attenuation curve (Finger and King 1978).

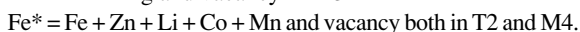
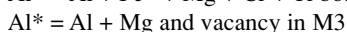
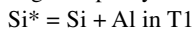
Least-squares refinement was made with the SHELX-93 program (Sheldrick 1993). Anisotropic atomic displacement parameters were allowed to vary for staurolite in air, whereas isotropic atomic displacement parameters were used for high-

**TABLE 1.** Lattice parameters of staurolite at various pressures

$P$ (GPa)	$a$ (Å)	$b$ (Å)	$c$ (Å)	$\beta$ (°)	$V$ (Å <sup>3</sup> )
<b>Sample I</b>					
1E-4	7.8720(4)	16.6245(3)	5.6606(7)	90.072(6)	740.79(9)
0.048(6)	7.8722(3)	16.6230(9)	5.6598(6)	90.069(6)	740.64(9)
2.230(5)	7.8421(2)	16.5588(2)	5.6370(7)	90.074(4)	731.99(6)
2.375(4)	7.8409(3)	16.5546(8)	5.6351(3)	90.075(6)	731.46(6)
3.930(6)	7.8199(6)	16.5092(8)	5.620(1)	90.06(1)	725.6(2)
5.969(6)	7.7949(4)	16.4565(5)	5.6011(8)	90.073(7)	718.4(1)
<b>Sample II</b>					
3.195(6)	7.8295(3)	16.5313(4)	5.6269(6)	90.074(6)	728.31(8)
5.781(7)	7.7965(4)	16.4608(5)	5.6015(7)	90.070(6)	718.88(9)
6.680(8)	7.786(4)	16.4385(5)	5.5941(8)	90.079(7)	715.9(1)
7.264(6)	7.779(3)	16.4239(3)	5.5886(7)	90.076(6)	714.01(9)

pressure refinements. Scattering factors for neutral atoms and correction factors for anomalous dispersion were taken from *International Tables for X-ray Crystallography* (Ibers and Hamilton 1974).

The dominant X-ray scattering cations in staurolite are Al, Si, Mg, and Fe. Because Al, Si, and Mg scatter X-rays in a very similar fashion, to reduce the number of variables we grouped these species together. With regard to elements with lower concentration, these were considered together with the main species, according to the cation partitioning proposed by Hawthorne et al. (1993a). In particular, we employed the following occupancy scheme in the refinements:



Details of refinement and data collection are listed in Table 2. The different numbers of reflections collected at different pressures are due to the casual overlapping of diffraction effects coming from the different parts of the DAC. In the refinements at 2.48 and 4.15 GPa, the isotropic thermal motion of M4 and the occupancy of T2 were blocked to avoid divergence problems.

Systematic errors may be introduced when a structural model obtained with diffraction from the whole reciprocal space is compared with results derived from limited portions of the reciprocal space. Therefore, we refined the structural model at room conditions selecting only the reflections accessible also with the DAC. A comparison of the geometrical results obtained with all data and with the selected ones shows slightly discrepant values for only a few bonds and the difference is of the same order of magnitude as the estimated standard deviations.

The atomic positions and electron number resulting from the refinement as shown in Table 3. Observed and calculated structure factors are listed in Table 4<sup>1</sup>.

<sup>1</sup>For a copy of Table 4, document item AM-02-013, contact the Business Office of the Mineralogical Society of America (see inside front cover of recent issue) for price information. Deposit items may also be available on the American Mineralogist web site at <http://www.minsocam.org>.

## RESULTS

### Ambient conditions

Refinement of intensity data collected at ambient condition was done in the *C2/m* space group using 2254 measured reflections, 1105 independent reflections, with resulting  $R_{\text{eq}} = 2.7\%$ , and  $R = 3.3\%$ . Our data agree perfectly with the results of Hawthorne et al. (1993a). However, because of the almost equal values of  $I(hkl)$  and  $I(h\bar{k}l)$ , the angle  $\beta$  value close to  $90^\circ$ , and the quasi-identity of the A and B sites of the monoclinic structure, isotropic refinement also was carried out in the higher symmetry space group, *Ccmm*. This procedure allows better comparison with high-pressure refinements, which were all carried out in the orthorhombic system due to the smaller number of data available at high  $P$ , owing to the lower number of accessible and measurable reflections in a DAC.

A statistical test (Hamilton 1965) shows that the increment of  $R$  in passing from monoclinic to orthorhombic symmetry is largely significant with data collected under room condition. In contrast, because of the reduced number of observations with the crystal in the DAC, the small decrease of  $R$  in passing from *Ccmm* to *C2/m* does not appear to be significant. This result supports the choice of refining staurolite at high pressure in the pseudo-orthorhombic system, with a smaller number of parameters.

Details of data collection and refinements in both monoclinic and orthorhombic systems are listed in Table 2. In the following tables, data at ambient conditions refer only to the refinement in the orthorhombic system.

### High- $P$

Variations with  $P$  of the lattice parameters  $a$ ,  $b$ ,  $c$ , and  $V$  (Table 1) are shown in Figure 2. The angle  $\beta = 90.07^\circ$  is not shown because it does not vary as a function of pressure. Volume-pressure data were fitted with a third-order Birch-Murnaghan EoS. The resulting EoS parameters are  $V_0 = 740.85(7) \text{ \AA}^3$  (very close to the measured value, Table 1,  $K_0 = 180(2) \text{ GPa}$ , and  $K' = 4.7(6)$ ).

A plot of the "normalized stress" defined as  $F_E = P/[3f_E(1+2f_E)^{5/2}]$  vs. the finite strain  $f_E = [(V_0/V)^{2/3} - 1]/2$  obtained from the  $P$ - $V$  data is linear (Fig. 3), shows that a 2<sup>nd</sup>-order truncation of the EoS could describe adequately the measured data. These results may be compared with those obtained by Grevel et al. (1998) for a synthetic Mg-staurolite, using multi-anvil

TABLE 2. Details of data collection and refinement at various pressures

$P$ (GPa)	Sample II					Sample III	
	0.0001	0.0001	2.48	4.15	5.43	6.84	8.74
$a$ (Å)	7.870(3)	7.886(2)	7.848(4)	7.820(5)	7.814(4)	7.792(5)	7.779(5)
$b$ (Å)	16.626(3)	16.659(4)	16.580(8)	16.510(9)	16.480(8)	16.465(9)	16.416(8)
$c$ (Å)	5.662(3)	5.671(1)	5.641(2)	5.626(3)	5.617(3)	5.599(3)	5.586(2)
$\beta$ (°)	90.06(2)						
Space group	<i>C2/m</i>	<i>Ccmm</i>	<i>Ccmm</i>	<i>Ccmm</i>	<i>Ccmm</i>	<i>Ccmm</i>	<i>Ccmm</i>
$\theta$ range	0–30	0–30	0–35	0–35	0–35	0–40	0–40
Scan type	$\omega$						
Scan width	2.0	2.0	2.0	2.0	2.0	2.0	2.0
No. measured refl.	2254	2254	435	421	456	609	730
No. independent refl.	1105	642	147	180	140	214	236
No. observed refl.	971	630	144	180	140	179	170
No. refined par.	114	33	31	31	33	33	33
$R$ equiv. %	2.7	2.6	3.7	5.5	6.2	4.4	4.7
Final $R$ % [ $> 4\sigma(I)$ ]	3.3	5.0	3.9	5.4	4.4	6.8	6.0

**TABLE 3.** Number of electrons assigned to each site, fractional atomic coordinates and  $U_{eq}/U_{iso}$  ( $\text{\AA}^2$ ) at various pressures

	$\Sigma e^-$	$x$	$y$	$z$	$U_{eq}/U_{iso}$
T1	14	0.13406(2)	0.1660(1)	1/4	0.0072(4)
		0.1333(4)	0.1665(4)	1/4	0.0061(9)
		0.1339(4)	0.1661(3)	1/4	0.0071(9)
		0.1342(6)	0.1667(5)	1/4	0.006(1)
		0.1335(5)	0.1668(4)	1/4	0.0046(9)
T2	21.3(3)	0.1336(4)	0.1665(3)	1/4	0.0069(8)
		0.3925(3)	0	1/4	0.0173(8)
		0.3927(4)	0	1/4	0.021(1)
		0.3925(5)	0	1/4	0.021(1)
		0.3926(5)	0	1/4	0.016(2)
M1	13	0.3935(5)	0	1/4	0.016(1)
		0.3935(5)	0	1/4	0.018(1)
		1/2	0.1752(1)	0	0.0077(4)
		1/2	0.1755(4)	0	0.0047(9)
		1/2	0.1757(4)	0	0.006(1)
M2	13	1/2	0.1757(6)	0	0.008(1)
		1/2	0.1760(6)	0	0.008(1)
		1/2	0.1752(4)	0	0.009(1)
		0.2633(3)	0.4105(1)	1/4	0.0086(5)
		0.2636(4)	0.4099(5)	1/4	0.007(1)
M3	6.4(2)	0.2636(5)	0.4100(4)	1/4	0.010(1)
		0.2631(6)	0.4103(6)	1/4	0.009(1)
		0.2638(5)	0.4105(5)	1/4	0.009(1)
		0.2637(4)	0.4098(4)	1/4	0.0089(9)
		0	0	0	0.008(2)
M4	1.0(2)	0	0	0	0.008(4)
		0	0	0	0.005(4)
		0	0	0	0.009(6)
		0	0	0	0.009(5)
		0	0	0	0.006(4)
O1	8	0.02(2)	0	0	0.02(2)
		0.001*	0	0	0.001*
		0.005*	0	0	0.005*
		0.06(7)	0	0	0.06(7)
		0.04(4)	0	0	0.04(4)
O2	8	0.001(2)	0	0	0.001(2)
		0.2349(6)	0	0.9658(9)	0.0105(9)
		0.2342(9)	0	0.966(2)	0.009(2)
		0.235(1)	0	0.968(1)	0.012(2)
		0.235(1)	0	0.968(2)	0.009(2)
O3	8	0.236(1)	0	0.969(2)	0.011(2)
		0.238(1)	0	0.970(1)	0.009(2)
		0.2550(4)	0.1613(2)	0.0153(6)	0.0084(6)
		0.2544(6)	0.1623(7)	0.015(1)	0.005(1)
		0.2540(8)	0.1603(6)	0.0147(9)	0.010(1)
O4	8	0.2558(9)	0.1630(7)	0.014(1)	0.003(2)
		0.2552(8)	0.1629(8)	0.014(1)	0.003(1)
		0.2546(6)	0.1614(7)	0.0137(9)	0.007(1)
		0.0016(7)	0.0891(3)	1/4	0.0107(9)
		0.0021(9)	0.0892(9)	1/4	0.005(2)
O5	8	0.002(1)	0.0889(9)	1/4	0.009(2)
		0.001(1)	0.087(1)	1/4	0.003(2)
		0.0018(9)	0.087(1)	1/4	0.003(2)
		0.0019(9)	0.08970(8)	1/4	0.003(2)
		0.0213(6)	0.2492(3)	1/4	0.0086(8)
O6	8	0.0219(9)	0.2489(9)	1/4	0.004(2)
		0.022(1)	0.2493(9)	1/4	0.009(2)
		0.018(1)	0.247(2)	1/4	0.007(2)
		0.016(1)	0.246(1)	1/4	0.005(2)
		0.017(1)	0.2472(9)	1/4	0.009(2)
O7	8	0.5268(6)	0.1001(3)	1/4	0.0083(9)
		0.5263(8)	0.1010(9)	1/4	0.006(2)
		0.5276(9)	0.1006(9)	1/4	0.008(2)
		0.527(1)	0.100(1)	1/4	0.006(2)
		0.526(1)	0.099(1)	1/4	0.004(2)
0.5237(9)	0.098(1)	1/4	0.007(2)		

Notes: From the uppermost values to the lowest ones the atomic coordinates coming from the refinements at 0.0001, 2.48, 4.15, 5.43, 6.84 and 8.74 GPa are reported. Estimated standard deviations refer to the last digit.

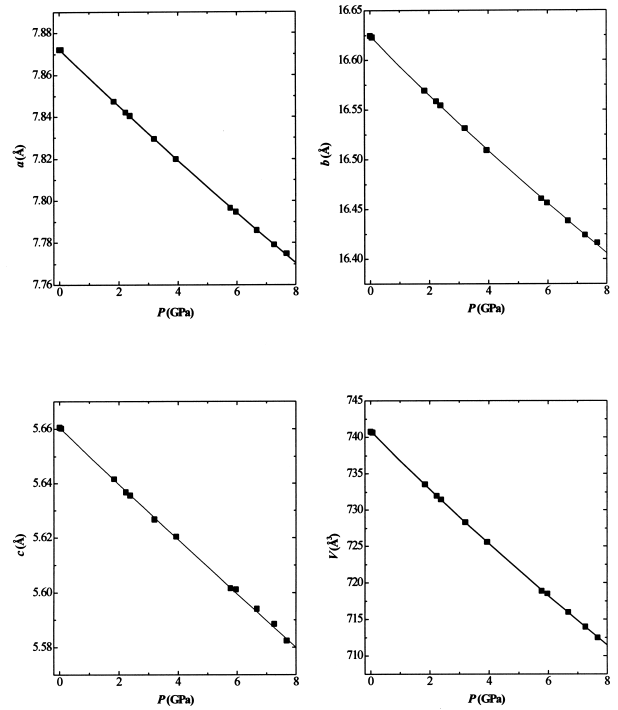


**FIGURE 2.** Variation of lattice parameters of staurolite as a function of pressure. Solid curves represent the Birch-Murnaghan EoS best fit. Note that the angle  $\beta$  is not reported because it remains constant in the investigated pressure range. Estimated standard deviations are smaller than the symbol size.

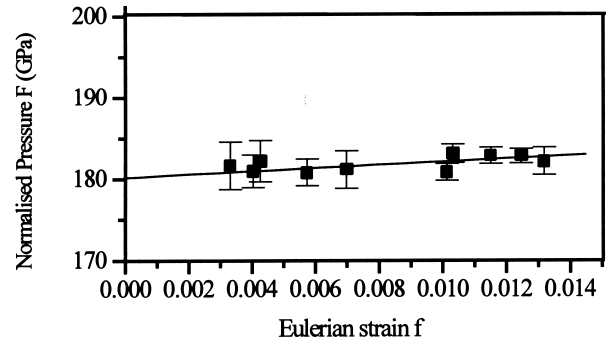


**FIGURE 3.** Plot of the “normalized stress,” defined as  $F_E = P/[3f_E(1+2f_E)^{3/2}]$ , vs. the finite strain  $f_E = [(V_0/V)^{2/3} - 1]/2$ .

X-ray apparatus. Those authors obtained a bulk modulus of 168.44(3.29) GPa with  $K' = 4$ . We obtained a bulk modulus of 182.7(6) GPa fixing  $K' = 4$  for our data.

Because the angle  $\beta$  does not vary as a function of pressure, the axial compressibilities have been obtained by fitting a third-order Birch-Murnaghan EoS to the cube of the lattice parameters. The results are:  $a_0 = 7.8723(2) \text{ \AA}$ ,  $K_0 = 189(2) \text{ GPa}$ ,  $K'_a = 4.1(6)$ ,  $b_0 = 16.62453(1) \text{ \AA}$ ,  $K_0 = 179(2) \text{ GPa}$ ,  $K'_b = 6.1(6)$ , and  $c_0 = 5.6604(4) \text{ \AA}$ ,  $K_0 = 179(5) \text{ GPa}$ , and  $K'_c = 2(1)$ . These values reveal a very isotropic behavior of staurolite with respect to the increase of pressure, as may be observed in dense

structures based on an oxygen close packing.

As the staurolite structure may be derived from that of both kyanite and spinel, the bulk moduli of all three may be expected to be similar. The bulk modulus of  $MgAl_2O_4$  spinel and its isomorph magnetite,  $Fe_3O_4$ , determined by Finger et al. (1986) as 194(6) and 186(5) GPa, respectively. The bulk moduli of kyanite measured by various authors are 172(3) GPa (Comodi et al. 1997), 193(1) GPa (Yang et al. 1997), and 183(4) GPa (Yagi et al. 1998). The small discrepancy observed in the kyanite bulk moduli may be correlated to the different pressure range investigated as well as to the different experimental procedures used. All these values are close to the bulk modulus of staurolite, as expected.

### Structural evolution with $P$

The evolution of the crystal structures of staurolite with  $P$ , obtained by comparison of structural refinements at 0.0001, 2.48, 4.15, 5.43, 6.84, and 8.74 GPa, may be described in terms both of evolution of single polyhedra and of the evolution of larger structural modules, involving groups of different polyhedra.

**Single-polyhedron evolution.** Table 5 lists the variations of all bond distances with  $P$ , together with the variations of polyhedral volumes and distortion parameters (Robinson et al. 1971). Figure 4 shows the evolution with  $P$  of the mean polyhedral bond distances, normalized to the ambient condition value.

A linear fit was used as a first approximation to describe the variation of the volume for each polyhedron as a function of pressure, due to the small number of data points. The bulk moduli were therefore calculated as the reciprocal of the mean compressibility coefficients obtained from the fits. The results show that the T1 tetrahedra occupied by Si are incompressible in the pressure range investigated, as already observed in several silicate structures (Hazen and Finger 1982 and references therein), whereas the T2 tetrahedra, partially occupied by Fe, has a bulk modulus of 104(6) GPa. The M1 and M2 octahedra, occupied by Al, are incompressible, whereas M3 and M4, partially occupied principally by Fe, have bulk moduli of 148(8) and 155(8) GPa, respectively. So, polyhedral evolution strongly depends not only on cation type, but also on the vacancy content.

Hazen and Finger (1978) observed that, in structures such as olivine and garnet, the cation polyhedra become more regular with increasing pressure because longer metal-oxygen bonds compress more than shorter ones. The same authors, on the basis of the results from several studies, later concluded that no general trends really exist in the variations of polyhedral distortion with  $P$  (Hazen and Finger 1982). For staurolite polyhedra, we determined deviations from regular geometric forms using distortion parameters, quadratic elongation  $\langle\lambda\rangle$ ,

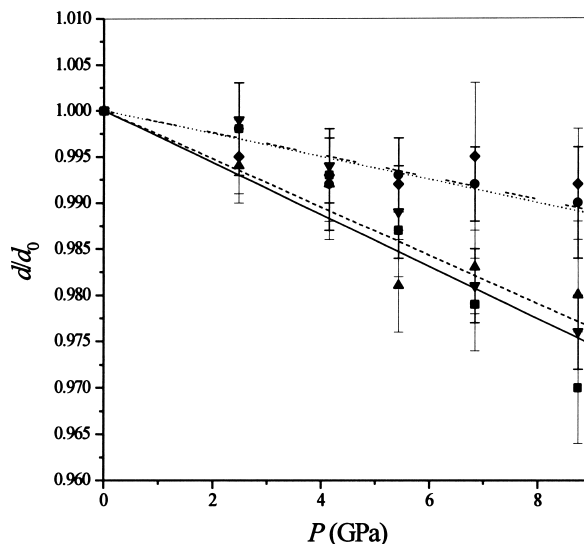


**FIGURE 4.** Mean polyhedral bond distances normalized to room condition value vs. pressure. Solid squares and line refer to T2, down and up triangles refer to M4 and M3 octahedra respectively. Dashed line represents the trend line for both octahedra. Full circles and dot line refer to M2, open diamonds and segment-dash lines refer to M1. T1 data are not reported because they remain almost unchanged in the  $P$  range investigated.

**TABLE 5.** Values of bond distances ( $\text{\AA}$ ), volumes ( $\text{\AA}^3$ ), distortion parameters (following Robinson et al. 1971) of polyhedra with pressure

$P$ (GPa)	0.0001	2.48	4.15	5.43	6.84	8.74
T1-O2( $\times 2$ )	1.639(4)	1.633(6)	1.626(6)	1.633(6)	1.629(6)	1.623(5)
T1-O4	1.647(5)	1.622(13)	1.632(15)	1.605(23)	1.597(19)	1.604(15)
T1-O3	1.653(6)	1.644(12)	1.641(15)	1.678(17)	1.661(17)	1.659(13)
<T1-O>	1.644(5)	1.633(10)	1.631(12)	1.637(15)	1.629(14)	1.627(11)
VT1	2.28(2)	2.23(4)	2.23(4)	2.25(6)	2.22(5)	2.21(5)
$\lambda$	1.000	1.000	1.000	1.001	1.001	1.001
$\sigma$	1.4	0.9	1.8	2.5	3.1	3.3
T2-O1( $\times 2$ )	2.035(5)	2.027(9)	2.007(9)	2.002(11)	1.997(10)	1.979(8)
T2-O5( $\times 2$ )	1.976(5)	1.975(14)	1.973(15)	1.954(21)	1.929(18)	1.909(15)
<T2-O>	2.005(5)	2.001(12)	1.990(12)	1.978(16)	1.963(14)	1.944(12)
VT2	4.13(3)	4.09(6)	4.03(6)	3.96(8)	3.87(7)	3.76(6)
$\lambda$	1.003	1.003	1.003	1.003	1.003	1.003
$\sigma$	11.3	14.1	11.5	11.8	11.9	13.6
M1-O5( $\times 2$ )	1.903(4)	1.886(12)	1.889(13)	1.886(18)	1.902(17)	1.888(13)
M1-O4( $\times 2$ )	1.903(4)	1.895(11)	1.883(12)	1.901(19)	1.900(17)	1.895(12)
O2( $\times 2$ )	1.948(3)	1.942(5)	1.945(7)	1.921(7)	1.921(7)	1.924(5)
<M1-O>	1.918(8)	1.908(9)	1.906(11)	1.903(15)	1.908(14)	1.902(10)
VM1	9.17(4)	9.1(1)	9.0(1)	9.0(2)	9.1(2)	9.0(1)
$\lambda$	1.010	1.013	1.015	1.011	1.010	1.010
$\sigma$	45.9	45.5	51.4	38.8	34.8	35.7
M2-O5	1.874(5)	1.871(8)	1.856(9)	1.856(11)	1.855(10)	1.872(9)
M2-O3	1.879(6)	1.872(7)	1.869(8)	1.860(9)	1.855(8)	1.854(7)
M2-O1( $\times 2$ )	1.929(4)	1.928(8)	1.927(8)	1.919(9)	1.915(9)	1.924(7)
M2-O2( $\times 2$ )	1.928(4)	1.921(10)	1.895(9)	1.917(11)	1.914(11)	1.886(9)
<M2-O>	1.911(5)	1.907(8)	1.895(9)	1.898(10)	1.895(10)	1.891(8)
VM2	9.08(5)	9.1(1)	8.9(1)	8.9(1)	8.9(1)	8.8(1)
$\lambda$	1.010	1.013	1.014	1.013	1.012	1.012
$\sigma$	44.2	44.1	45.7	41.8	38.3	40.9
M3-O1( $\times 2$ )	1.863(5)	1.848(7)	1.853(8)	1.850(10)	1.848(10)	1.857(8)
M3-O3( $\times 4$ )	2.053(4)	2.043(10)	2.035(12)	2.003(14)	2.010(14)	1.998(10)
<M3-O>	1.990(5)	1.978(9)	1.974(10)	1.952(12)	1.956(12)	1.951(9)
VM3	10.36(6)	10.2(1)	10.2(1)	9.8(1)	9.9(1)	9.8(1)
$\lambda$	1.008	1.008	1.007	1.006	1.006	1.005
$\sigma$	12.9	12.1	10.8	10.0	9.5	8.0
M4-O1( $\times 2$ )	2.099(5)	2.095(7)	2.078(8)	2.074(11)	2.064(10)	2.047(8)
M4-O5( $\times 4$ )	2.200(4)	2.199(13)	2.190(12)	2.176(19)	2.156(16)	2.146(13)
<M4-O>	2.166(5)	2.164(10)	2.153(10)	2.142(15)	2.125(13)	2.113(11)
VM4	12.93(6)	13.0(1)	12.7(1)	12.6(2)	12.3(2)	12.2(1)
$\lambda$	1.028	1.029	1.029	1.027	1.026	1.023
$\sigma$	85.2	85.9	86.8	81.3	77.8	69.4

and bond-angle variance  $\sigma^2$ , as defined by Robinson et al. (1971). The results (Table 5) show that, whereas it is impossible to observe any clear trend in tetrahedra, probably due to the large relative error, a clear trend toward regularity with pressure is present in the octahedra. In particular the softer octahedra, M3 and M4, show the greatest reduction in both quadratic elongation and bond angle distortion.

**Layer evolution.** Because the staurolite structure may be described as layers of kyanite and Fe-Al-oxide-hydroxide alternating along [010], it was of interest to examine the baric evolution of the single layers. Table 6 shows the evolution of the interoctahedral site distances with  $P$ . Table 7 lists the thickness of the two layers along the  $b$  axis at different values of pressure. The thickness of Fe-Al-oxide-hydroxide layer decreases from 3.096(6) to 3.018(9) Å between 0.0001 and 8.74 GPa, whereas that of the kyanite layer fell from 5.233(7) to 5.190(11) Å in the same pressure range. That is, the reduction of Fe-Al-oxide-hydroxide is three times that of the kyanite layer, the former decreasing by 2.5% and the latter by only 0.8%.

Looking at the reduction in layer volume, a smaller anisotropy stands out. The kyanite layer is reduced by 3.6% and in that of the Fe-Al-oxide-hydroxide layer by 5%. In terms of bulk moduli, we measured values of about 220(8) GPa for the kyanite layer and 150(6) GPa for the Fe-Al-oxide-hydroxide layer, whose average is in agreement with the value of the bulk modulus obtained for the unit-cell volume. This different behavior is a consequence of different charge distribution, as documented well by the transmission electron microscopy study of Downing et al. (1990). The three-dimensional Coulomb potential of the unit-cell of staurolite determined in that study revealed a complex surface with large cavities corresponding to the sites with partial occupancy. This difference in charge distribution could explain the good cleavage along the  $b$  axis (Deer et al. 1992).

## DISCUSSION

The thermal expansion of a synthetic end-member of Fe staurolite was determined by Gibbons et al. (1981), using the high-temperature XRD method. They found a linear increase in lattice parameters up to about 500 °C, when an abrupt increase in the parameters indicated that dehydroxylation of staurolite had occurred. By combining our high-pressure data with those of Gibbons et al. (1981), the following equation of state

may be formulated:  $V/V_0 = 1 + 1.78(9) 10^{-5} T - 4.99(5) 10^{-3} P$ , where temperature is expressed in °C and pressure in GPa. This equation is valid up to about 500 °C, but it gives only approximate values due to the assumptions that the pressure derivative of thermal expansion and the temperature derivative of compressibility are zero. Because of the many experimental difficulties, these terms have, in fact, only been measured in a few minerals (see Pavese et al. 2001). At present, it is difficult to describe general reliable trends regarding the effects of temperature on bulk modulus or of pressure on thermal expansion. However, for staurolite, the  $P$ - $V$ - $T$  data of Grevel et al. (1998), obtained using multi-anvil X-ray apparatus, show that the thermal expansion of a synthetic Mg-staurolite between 0 and 1000 °C does not vary for pressures between 0.7 GPa and 6.5 GPa.

Experimental petrological studies (Hellman and Green 1978; Poli and Schmidt 1995) indicate that staurolite is important in petrogenetic models of the mineralogical changes and melting processes occurring in Benioff zones. Therefore, the conditions for staurolite stability must be determined if the hypothesis is to be confirmed. An important key to study the evolution of Earth's mantle is the determination of isochors, which allow us to fix the  $P$ - $T$  conditions at which a structure is volume-invariant. For staurolite, a gradient of 35 bar/°C was calculated with the above equation. As a consequence, a geothermal gradient of about 10 °C/Km may be calculated, corresponding to gradients commonly found in medium-high pressure metamorphism, i.e., blueschist facies.

Pressure-temperature-time ( $P$ - $T$ - $t$ ) paths in subduction zones depend on several variables that change in different subduction zones (Peacock 1990). The most important factors are the age of the incoming lithosphere, the location of the rock in the subduction zone, and the vigor of convection in the mantle wedge. Subduction zones, forming in young and relatively hot oceanic lithosphere, give warmer slab  $P$ - $T$ - $t$  paths than those forming in older oceanic lithosphere. The volume-invariant conditions found for staurolite (10 °C/Km) fit very well with the conditions determined for warmer slabs. Other hydrous minerals, such as lawsonite and epidote, have a similar volume invariance gradient (Comodi and Zanazzi 1996, 1997). On the other hand, kyanite and magnesiochloritoid with a gradient of 7 °C/Km (Comodi et al. 1997, 1992), may be stable in colder slabs.

Generally several studies on structural evolution with temperature and pressure of hydrous phases—epidote, lawsonite, magnesiochloritoid, and staurolite—define the range of  $P$ - $T$  conditions found in various regimes in subducting slabs. In this way, data from experimental mineralogy, although from a different point of view, do fit data from experimental petrology (Poli and Schmidt 1995) on the possibility of carrying fluids in the kinds of  $P$ - $T$  regimes found in Benioff zones. In particular,

Comodi et al. (2000) have used the experimental equations of state of these hydrous phases to reproduce the assemblages and to model a wide range of bulk compositions involved in the subduction zones. Experimental and computed results show that chloritoid- and lawsonite-bearing as-

**TABLE 6.** Inter-octahedral site distances at various pressures

$P$ (GPa)	0.0001	2.48	4.15	5.43	6.84	8.74
M1-M1	2.836(1)	2.82(1)	2.81(1)	2.81(1)	2.78(1)	2.79(1)
M1-M2	2.892(2)	2.88(1)	2.87(1)	2.86(2)	2.87(2)	2.85(1)
M2-M3	2.778(2)	2.77(2)	2.76(1)	2.75(2)	2.74(1)	2.74(1)
M1-M4	2.919(2)	2.91(2)	2.91(2)	2.89(2)	2.90(2)	2.88(2)
M2-M4	2.923(2)	2.91(2)	2.91(1)	2.89(2)	2.89(1)	2.89(1)
M3-M3	2.836(1)	2.82(1)	2.81(1)	2.81(1)	2.80(1)	2.79(1)
M4-M4	2.836(1)	2.82(1)	2.81(1)	2.81(1)	2.80(1)	2.79(1)

**TABLE 7.** Evolution with  $P$  of the thickness along  $b$  and of the volumes of the hydroxyl and kyanite layers

$P$ (GPa)	0.0001	2.48	4.15	5.43	6.84	8.74
$\Delta b$ hydroxyl layer (Å)	3.096(6)	3.097(8)	3.083(8)	3.036(9)	3.028(8)	3.018(9)
$\Delta b$ kyanite layer (Å)	5.233(7)	5.193(9)	5.192(10)	5.195(10)	5.207(11)	5.190(11)
$V$ hydroxyl layer (Å <sup>3</sup> )	138.5(2)	137.1(4)	136.3(4)	133.3(5)	132.1(5)	131.1(5)
$V$ kyanite layer (Å <sup>3</sup> )	234.0(3)	229.9(5)	228.6(5)	228.0(6)	227.2(6)	225.5(6)

semblage are restricted to mature, nearly steady-state, subducted zones, whereas staurolite and epidote are hydrous phases stable in a wide range of orogenic settings when relatively warmer environments develop.

An early attempt to predict crystal bulk moduli by an empirical equation was made by Bridgman (1923), who found a relationship between compressibility and molar volumes in about 30 metals. Later, Anderson (1972) also proposed the constancy of the product between bulk modulus and molar volume for isostructural materials.

The present data on staurolite, together with data from the literature on magnesiochloritoid, ellenbergerite, clinopyroxene, lawsonite, epidote, and kyanite (Comodi et al. 1992; Comodi and Zanazzi, 1993b; Comodi et al. 1995; Comodi and Zanazzi 1996; Comodi and Zanazzi 1997; Comodi et al. 1997) represent a homogeneous set of compressibility data obtained from single-crystal studies. All these minerals have close-packed structures. The atomic packing efficiency of a mineral may be expressed by the ratio between the volume occupied by one oxygen atom with radius equal to 1.315 Å and that occupied by one oxygen atom in the mineral (Comodi and Zanazzi 1993b). If we show the bulk moduli of the above minerals with respect to the volume occupied by one oxygen ( $V_{Ox}$ ) in the form of a diagram, we find a very good trend, as shown in Figure 5. The bulk moduli- $V_{Ox}$  relationship may be tentatively used to predict the compressibility of solids with structures based on close packing of oxygen atoms. However, this procedure does not work for structures in which mechanisms such as polyhedral tilting make an important contribution to the high-pressure evolution of the structure, or when large-scale anisotropy occurs in the charge distribution. As examples, data for amphiboles and micas (Comodi et al. 1991; Comodi and Zanazzi

1995) are also reported in Figure 5. These points are quite far from the trend, due to the combination of various mechanisms in determining bulk moduli.

## ACKNOWLEDGMENTS

Many thanks are due to late L. Ungaretti for supplying samples; to his memory this paper is dedicated. High-pressure diffraction experiments were performed at the Bayerisches Geoinstitut under the EU "IHP-Access to Research Infrastructures" programme (Contract No. HPRI-1999-CT-00004 to D.C. Rubie) and at Dipartimento di Scienze della Terra, University of Perugia (Italy) under the project "Transformations, reactions, ordering in minerals," supported by CNR and MURST, grants to P.F.Z. G. Walton revised the English text.

## REFERENCES CITED

- Anderson, O.L. (1972) In E.C. Robinson, Ed., *Nature of the Solid Earth. Patterns in elastic constants of minerals important to geophysics*. McGraw-Hill, New York, 575–613.
- Andersson, S. and Hyde, B.G. (1982) An attempted exact, systematic geometrical description of crystal structures. *Zeitschrift für Kristallographie*, 158, 119–131.
- Angel, R.J., Allan, D.R., Miletich, R., Finger, L.W. (1997) The use of quartz as an internal pressure standard in high pressure crystallography. *Journal of Applied Crystallography*, 30, 461–466.
- Bridgman, P.W. (1923) The compressibility of thirty metals as a function of temperature and pressure. *Proceedings of the American Academy of Arts and Sciences*, 58, 165–172.
- Caucia, F., Callegari, A., Oberti, R., Ungaretti, L., and Hawthorne, F. (1994) Structural aspects of oxidation-dehydrogenation in staurolite. *Canadian Mineralogist*, 32, 477–489.
- Comodi, P. and Zanazzi, P.F. (1993a) Improved calibration curve for the  $Sm^{2+}$ , BaFCl pressure sensor. *Journal of Applied Crystallography*, 26, 843–845.
- (1993b) Structural study of ellenbergerite. Part II: Effects of high pressure. *European Journal of Mineralogy*, 5, 831–838.
- (1995) High pressure structural study of muscovite. *Physics and Chemistry of Minerals*, 22, 170–177.
- (1996) Effects of temperature and pressure on the structure of lawsonite. *American Mineralogist*, 81, 833–841.
- (1997) The pressure behavior of clinozoisite and zoisite: an X-ray diffraction study. *American Mineralogist*, 82, 61–68.
- Comodi, P., Mellini, M., Ungaretti, L., and Zanazzi, P.F. (1991) Compressibility and high-pressure structure refinement of tremolite, pargasite and glaucophane. *European Journal of Mineralogy*, 3, 485–499.
- Comodi, P., Mellini, M., and Zanazzi, P.F. (1992) Magnesiochloritoid, compressibility and high pressure structure refinement. *Physics and Chemistry of Minerals*, 18, 483–490.
- Comodi, P., Melacci, P.T., Polidori, G., and Zanazzi, P.F. (1994) Trattamento del profilo di diffrazione da campioni in cella ad alta pressione. *Proceedings of XXIV National Congress of Associazione Italiana di Cristallografia*. Pavia, September 27–29, 119–120. Italy.
- Comodi, P., Princivalle, F., Tirone, M., and Zanazzi, P.F. (1995) Comparative compressibility of clinopyroxenes from mantle nodules. *European Journal of Mineralogy*, 7, 141–149.
- Comodi, P., Zanazzi, P.F., Poli, S., and Schmidt, M.W. (1997) High-pressure behavior of kyanite: Compressibility and structural deformations. *American Mineralogist*, 82, 452–459.
- Comodi, P., Poli, S., and Zanazzi, P.F. (2000) Hydrous phases in subducting slabs: evidences from experimental mineralogy. *Evoluzione Geologica e Geodinamica dell'Appennino*. Conference Abstract, 98–99.
- Denner, W., Schultz, H., and d'Amour, H. (1978) A new measuring procedure for data collection with a high-pressure cell on X-ray four-circle diffractometer. *Journal of Applied Crystallography*, 11, 260–264.
- Deer, W.A., Howie, R.A., and Zussman, J. (1992) *An introduction to the rock-forming minerals*, p. 696. Longman, Burnt Mill, Harlow, England.
- Downing, K.H., Meisheng, H., Wenk, H.R., and O'Keefe, M.A. (1990) Resolution of oxygen atoms in staurolite by three-dimensional transmission electron microscopy. *Nature*, 348, 525–528.
- Finger, L.W. and King, H. (1978) A revised method of operation of the single crystal diamond cell and refinement of the structure of NaCl at 32 kbar. *American Mineralogist*, 63, 337–342.
- Finger, L.W., Hazen, R.M., and Hofmeister, A.M. (1986) High-pressure crystal chemistry of spinel ( $MgAl_2O_4$ ) and magnetite ( $Fe_3O_4$ ): Comparison with silicate spinels. *Physics and Chemistry of Minerals*, 13, 215–220.
- Ganguly, J. (1972) Staurolite stability and related parageneses: Theory, experiments, and applications. *Journal of Petrology*, 13, 335–365.
- Gibbons, K., Dempsey, M.J., and Henderson, C.M.B. (1981) The thermal expansion of staurolite,  $Fe_2Al_6Si_4O_{44}(OH)_2$ . *Mineralogical Magazine*, 44, 69–72.
- Gibson, G.M. (1978) Staurolite in amphibole and hornblende sheets from the Upper Seaforth River, central Fiordland, New Zealand. *Mineralogical Magazine*,

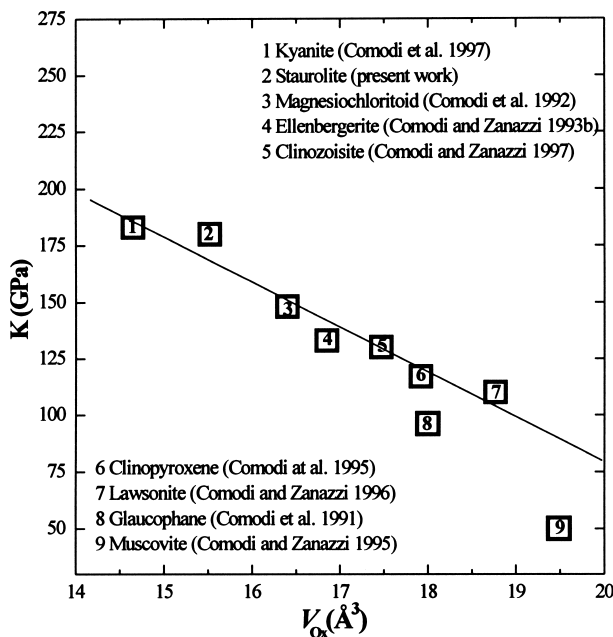


FIGURE 5. Bulk moduli vs. volume occupied by an oxygen atom in some minerals with structure roughly based on close packing of oxygen atoms.

- 42, 153–154.
- Grevel, K.D., Fasshauer, D.W., and Rohling, S. (1998) P-V-T data of kyanite and Mg-staurolite for pressures up to 7.5 Gpa. *Terra Abstract*, 1, 23.
- Hamilton, W.C. (1965) Significance tests on the crystallographic *R* factor. *Acta Crystallographica*, 18, 502–510.
- Hawthorne, F.C., Ungaretti, L., Oberti, R., Caucia, F., and Callegari, A. (1993a) The crystal chemistry of staurolite. I. Crystal structure and site populations. *Canadian Mineralogist*, 31, 551–582.
- (1993b) The crystal chemistry of staurolite. II. Order-disorder and the monoclinic → orthorhombic phase transition. *Canadian Mineralogist*, 31, 583–595.
- (1993c) The crystal chemistry of staurolite. III. Local order and chemical composition. *Canadian Mineralogist*, 31, 597–616.
- Hazen, R.M. and Finger, L.W. (1978) Crystal structures and compressibilities of pyrope and grossular to 60 kbar. *American Mineralogist*, 63, 297–303.
- (1982) *Comparative crystal chemistry*, p. 230. Wiley, New York.
- Hellman, P.L. and Green, T.H. (1978) The high pressure experimental crystallisation of staurolite in hydrous mafic compositions. *Contributions to Mineralogy and Petrology*, 68, 369–372.
- Ibers, J.A. and Hamilton, W.C., Eds. (1974) *International Tables for X-ray Crystallography* vol. 4, 366 p. Kynoch Press, Birmingham, U.K.
- Koch-Müller, M., Langer, K., and Beran, A. (1995) Polarized single-crystal FTIR-spectra of natural staurolite. *Physics and Chemistry of Minerals*, 22, 108–114.
- Koch-Müller, M., Kahlenberg, V., Bubenick, W., and Gottschalk, M. (1998) Crystal-structure refinement of synthetic Fe- and Mg-staurolite by Rietveld analysis of X-ray powder-diffraction data. *European Journal of Mineralogy*, 10, 453–460.
- Koch-Müller, M., Wumbach, I.A., and Bubenick, W. (1999) Intracrystalline fractionation of Fe in synthetic (Fe, Mg, Zn)-bearing staurolite: a Mössbauer spectroscopic study. *Physics and Chemistry of Minerals*, 26, 312–321.
- Náray-Szabó, I. (1929) The structure of staurolite. *Zeitschrift für Kristallographie*, 71, 103–116.
- Náray-Szabó, I. and Sasvári, K. (1958) On the structure of staurolite  $\text{HF}_2\text{Al}_9\text{Si}_4\text{O}_{24}$ . *Acta Crystallographica*, 11, 862–865.
- Pavese, A., Diella, V., Pischedda, V., Merli, M., Bocchio, R., and Mezouar, M. (2001) Pressure-volume-temperature equation of state of andradite and grossular, by high-pressure and -temperature powder diffraction. *Physics and Chemistry of Minerals*, 28, 242–248.
- Peacock, S.M. (1990) Fluid processes in subduction zones. *Science*, 248, 329–337.
- Poli, S. and Schmidt, M.W. (1995)  $\text{H}_2\text{O}$  transport and release in subduction zones: Experimental constraints on basaltic and andesitic systems. *Journal of Geophysical Research*, 22, 299–22, 314.
- Ralph, R.L. and Finger, L.W. (1982) A computer-program for refinement of crystal orientation matrix and lattice-constant from diffractometer data with lattice symmetry constrains. *Journal of Applied Crystallography*, 15, 537–539.
- Richardson, S.W. (1966) The stability of Fe-staurolite + quartz. *Carnegie Institute of Washington Yearbook*, 66, 397–398.
- Robinson, K., Gibbs, G.V., and Ribbe, P.H. (1971) Quadratic elongation: a quantitative measure of distortion in coordination polyhedra. *Science*, 172, 567–570.
- Schreyer, W. (1988) Experimental studies on metamorphism of crustal rocks under mantle pressures. *Mineralogical Magazine*, 52, 1–26.
- Schreyer, W. and Chinner, G.A. (1966) Staurolite-quartzite band in kyanite-quartzite at Big Rock, Rio Arriba County, New Mexico. *Contribution to Mineralogy and Petrology*, 12, 223–244.
- Sheldrick, G.M. (1993) SHELX93, Program for crystal structure determination. University of Göttingen, Germany.
- Ståhl, K. and Legros, J.P. (1990) On the structure of staurolite. The X-ray crystal structure of staurolite from the Pyrenees and Brittany. *Acta Crystallographica*, B46, 292–301.
- Ståhl, K., Kvik, Å., and Smith, J.V. (1988) A neutron diffraction study of hydrogen positions at 13 K, domain model and chemical composition of staurolite. *Journal of Solid State Chemistry*, 73, 362–380.
- Yagi, T., Inutsuka, S., and Kondo, T. (1998) Isothermal compression curve of  $\text{Al}_2\text{SiO}_5$  kyanite. In *Properties of Earth and planetary materials at high pressure and temperature*. Geophysical Monograph, 101, 281–286.
- Yang, H., Downs, R.T., Larry, W., Finger, L.W., Hazen, R.M., and Prewitt, C.T. (1997) Compressibility and crystal structure of kyanite,  $\text{Al}_2\text{SiO}_5$ , at high pressure. *American Mineralogist*, 82, 467–474.

MANUSCRIPT RECEIVED SEPTEMBER 7, 2001

MANUSCRIPT ACCEPTED MARCH 17, 2002

MANUSCRIPT HANDLED BY YINGWEI FEI